Structure of the β-Amyloid$_{(10-35)}$ Fibril

Timothy S. Burkoth,[†] Tammie L. S. Benzinger,[‡] Volker Urban,[||] David M. Morgan,[†] David M. Gregory,[⊥] P. Thiyagarajan,[§] Robert E. Botto,[⊥] Stephen C. Meredith,[‡] and David G. Lynn*,[†]

Contribution from the Departments of Chemistry and Pathology, The University of Chicago, Chicago, Illinois 60637-1043, and Intense Pulse Neutron Source and Chemistry Division, Argonne National Laboratory, Argonne, Illinois 60439

Received February 22, 2000

Abstract: The primary component of the amyloid plaques in Alzheimer's disease (AD) is a highly ordered fibril composed of the 39−43 amino acid peptide, β-amyloid (Aβ). The presence of this fibril has been correlated with both the onset and severity of the disease. Using a combination of synthetic model peptides, solid-state NMR, electron microscopy, and small angle neutron scattering (SANS), methods that allowed fibrils to be studied directly both in solution and in the solid state, the three-dimensional structure of fibrils formed from A$\beta_{(10-35)}$ is assigned. The structure consists of six laminated β-sheets propagating and twisting along the fibril axis. Each peptide strand is oriented perpendicular to the helical axis in a parallel β-sheet, with each like amino acid residue in register along the sheet. The six sheets are laminated, probably also in parallel arrays, to give a fibril with dimensions of about 60 × 80 Å. Both the methodology developed and the structural insight gained here lay the foundation for strategies to characterize and design materials capable of amyloid-like self-assembly.

Introduction

Several widely different disorders, including Alzheimer's disease (AD), systemic amyloidosis, mature onset diabetes, and prion-transmissible spongiform encephalopathies, have now been grouped into the common category of amyloid diseases.[1] All have in common the abnormal folding of a normal soluble protein, or proteolytic product thereof, into a state which promotes self-association and aggregation. The self-assembly of these proteins manifests itself in the formation of well-organized paracrystalline fibrillar structures maintaining a dominant β peptide conformation.

The term paracrystallinity is imprecise, connoting any material that forms significant long-range order that is short of a three-dimensional crystal lattice. Many biopolymer materials show elements of paracrystallinity including collagen, deoxy-hemoglobin S fiber, actin, and tropomyosin, as well as some viral particles, cell surface structures, and intracellular inclusion bodies.[2] Over the last several years, divergent block copolymers forming tubular micelle-like aggregates that exhibit elements of paracrystallinity have been discovered.[3] It is both the long-range structural order and the favorable energetics of self-assembly of these rodlike materials that suggest great opportunities for the construction of nanoscale materials.[4] However, the amyloids pose serious structural assignment limitations, not only because of size and low solubility, but also because of the inherent symmetry of the repeating arrays. Consequently, the limited structural information has hampered both the development of therapies for the amyloid diseases and the insight needed to design and construct such materials.

The Aβ peptide associated with the pathogenesis of AD[5] is the most tractable of the amyloids, at least in terms of the small size of the aggregating entity. This 39−43 amino acid peptide, a proteolytic product of the amyloid precursor protein (β-APP),[6] has three notable regions: a hydrophilic N-terminus (aa 1−16),

* Address correspondence to current address: Emerson Hall, Departments of Chemistry and Biology, Emory University, Atlanta, GA 30322.
[†] Department of Chemistry, The University of Chicago.
[‡] Department of Pathology, The University of Chicago.
[||] Present address: ESRF, 38043 Grenoble Cedex, France.
[§] Intense Pulse Neutron Source, Argonne National Laboratory.
[⊥] Chemistry Division, Argonne National Laboratory.

(1) Sipe, J. D. *Annu. Rev. Biochem.* **1992**, *61*, 947−975. Teplow, D. *Int. J. Exp. Clin. Invest.* **1998**, *5*, 121−142.
(2) Knight, D. P.; Hunt, S. *Tissue Cell* **1976**, *8*, 183−93. Heine, H.; Schaeg, G. *Virchows Archiv A, Path. Anat. Hist.* **1977**, *376*, 89−94. Horne, R. W. *J. Microsc.* **1978**, *113*, 241−56. Magdoff-Fairchild, B.; Chiu, C. C. *Proc. Natl. Acad. Sci. U.S.A.* **1979**, *76*, 223−6. Ohtsuki, I.; Nagano, K. *Adv. Biophys.* **1982**, *15*, 93−130. Eaton, W. A.; Hofrichter, J. *Adv. Protein Chem.* **1990**, *40*, 63−279. Schroder, J. M. *Brain Path.* **1993**, *3*, 177−90. Kupcu, S.; Sleytr, U. B.; Sara, M. *J. Immunol. Meth.* **1996**, *196*, 73−84. Zhang, R.; Tristram-Nagle, S.; Sun, W.; Headrick, R. L.; Irving, T. C.; Suter, R. M.; Nagle, J. F. *Biophys. J.* **1996**, *70*, 349−57. Taylor, K. A.; Tang, J.; Cheng, Y.; Winkler, H. *J. Struct. Biol.* **1997**, *120*, 372−86. Zinkernagel, R. M. *Biol. Chem.* **1997**, *378*, 725−9. Bouchard, M.; Pare, C.; Dutasta, J. P.; Chauvet, J. P.; Gicquand, C.; Auger, M. *Biochemistry* **1998**, *37*, 3149−55. Ellis, M. J.; Knapp, S.; Koeck, P. J.; Fakoor-Biniaz, Z.; Ladenstein, R.; Hebert, H. *J. Struct. Biol.* **1998**, *123*, 30−6. Geisler, N.; Schunemann, J.; Weber, K.; Haner, M.; Aebi, U. *J. Mol. Biol.* **1998**, *282*, 601−17. Molnar, M.; Schroder, J. M. *Acta Neuropath.* **1998**, *96*, 41−51.
(3) Yu, Y.; Zhang, L.; Eisenberg, A. *Macromolecules* **1998**, *31*, 1144−54. Yamada, N.; Ariga, K.; Naito, M.; Matsubara, K.; Koyama, E. *J. Am. Chem. Soc.* **1998**, *120*, 12192−99. Won, Y.-Y.; Davis, H. T.; Bates, F. S. *Science* **1999**, *283*, 960−3. Kline, S. R. *Langmuir* **1999**, *15*, 2726−32.
(4) Burkoth, T. S.; Benzinger, T. L. S.; Urban, V.; Lynn, D. G.; Meredith, S. C.; Thiyagarajan, P. *J. Am. Chem. Soc.* **1999**, *121*, 7429−7430.
(5) Selkoe, D. J. *J. Neuropathol. Exp. Neurol.* **1994**, *53*, 438−447. Selkoe, D. J. *J. Biol. Chem.* **1996**, *271*, 18295−18298.
(6) Glenner, G. G.; Wong, C. W. *Biochem. Biophys. Res. Commun.* **1984**, *122*, 1131−35. Masters, C. L.; Simms, G.; Weinman, N. A.; Multhaup, G.; McDonald, B. L.; Beyreuther, K. *Proc. Natl. Acad. Sci. U.S.A.* **1985**, *82*, 4245−49. Kang, J.; Lemaire, H. G.; Unterbeck, A.; Salbaum, J. M.; Masters, C. L.; Grzeschik, K. H.; Multhaup, G.; Beyreuther, K.; Muller-Hill, B. *Nature* **1987**, *325*, 733−6. Prelli, F.; Castano, E.; Glenner, G. G.; Frangione, B. *J. Neurochem.* **1988**, *51*, 648−51. Vassar et al. *Science* **1999**, *286*, 735−41. Selkoe, D. J. *Nature* **1999**, *399*, A23−31.

10.1021/ja000645z CCC: $19.00
Published on Web 08/06/2000

^{1}DAEFRHDSG ^{10}YEVHHQK**LVFFA**EDVGSNK**GAIIGL**^{35}**MVGGVVI** ^{42}**A**

A$\beta_{(10\text{-}35)}$ ^{10}YEVHHQK**LVFFA**EDVGSNK**GAIIGL**^{35}**M**

Aβ-PEG ^{10}YEVHHQK**LVFFA**EDVGSNK**GAIIGL**^{35}**M**–NH–(CH$_2$CH$_2$O)$_x$–CH$_2$CH$_2$OH

A.

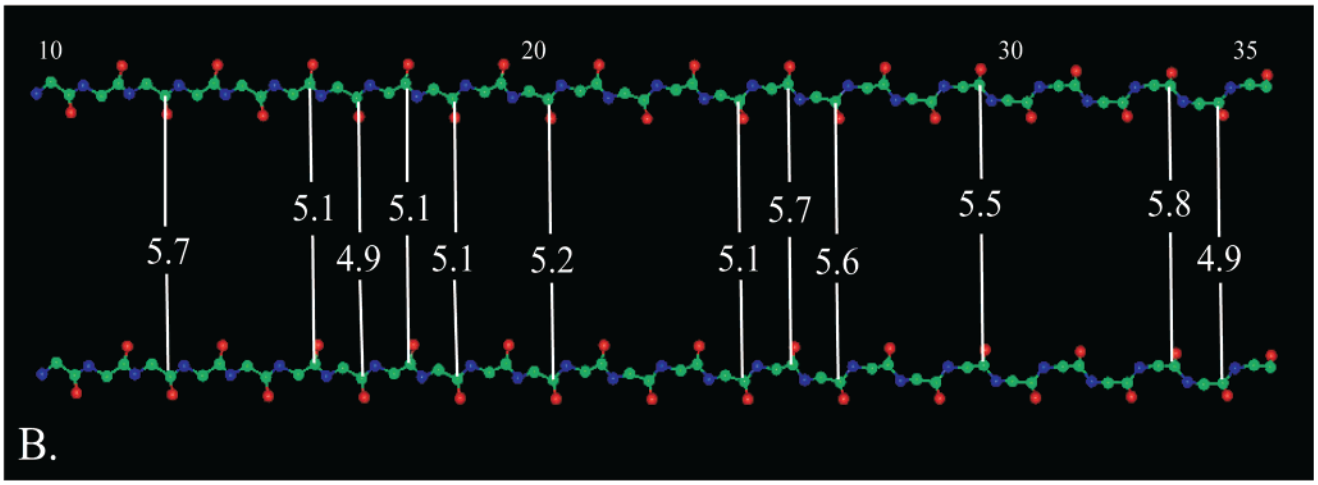

Figure 1. (A) The amino acid sequence of Aβ can be separated into distinct domains: a hydrophilic N-terminus (aa 1−16), a central hydrophobic region (aa 17−21), and a long hydrophobic C-terminus (aa 29−43). These domains are shown to be conserved in A$\beta_{(10-35)}$ and Aβ-PEG. (B) Summary of the inter peptide ^{13}C carbonyl contacts observed for A$\beta_{(10-35)}$ by solid-state NMR. Inter peptide distances were measured using DRAWS at positions V_{12}, Q_{15}-V_{18}, F_{20}, V_{24}-G_{26}, G_{29}, G_{33}, and L_{34}. Glycine residues and residues proximal to glycine exhibited larger distances and greater measurement error, ±0.4 Å, attributable to more flexibility or disorder. Likewise, the amino-terminal V_{12} exhibited considerable flexibility and a calculated distance of 5.7 ± 0.5 Å, but L_{34} showed a well-defined contact distance.

a central hydrophobic stretch (aa 17−21), and a long hydrophobic C-terminus (aa 29−43). A$\beta_{(10-35)}$, a peptide comprising the core residues 10−35, preserves these characteristic regions (Figure 1A) and has been shown to self-assemble into characteristic amyloid,[7a,b] but in more homogeneous fibrillar arrays.[7c−f] Dipolar recoupling solid-state NMR experiments[8] enabled precise inter-strand distance measurements at the backbone carbonyls of residues 12, 15−18, 20, 24, 25, 26, 29, 33, and 34, establishing that each peptide in the fibril is arrayed as a parallel β-strand, and in the extended sheet, each amino acid residue is in register with like residues in adjacent strands (Figure 1B).[7c−f]

This parallel β-sheet orientation clusters the hydrophobic C-terminus of each peptide along one face of the self-assembled array. A priori, such a solvent exposed hydrophobic surface propagating along one face would be expected to impact the solubility of the fibrils. To investigate this possibility, a poly(ethylene glycol) block was synthetically attached at the C-terminus of A$\beta_{(10-35)}$.[9] This A$\beta_{(10-35)}$-PEG block copolymer, Figure 1A, formed fibrils with greatly improved solubility. Most importantly, and unlike the native peptide, the formation of fibrils by A$\beta_{(10-35)}$-PEG was completely reversible, allowing the demonstration of a concentration-dependent equilibrium between the unstructured peptide and a β-strand hexamer during fibrillogenesis.[9] A$\beta_{(10-35)}$-PEG fibrils also rarely formed laterally associated tangled webs characteristic of the amyloids. It was concluded that the PEG moeity prevented lateral association of the fibrils and thereby inhibited the irreversible step in fibrilogenesis.[9] Here we exploit this opportunity to study both the reversibly self-associating block copolymer A$\beta_{(10-35)}$-PEG in solution and the amyloid fibril in the solid state to characterize the three-dimensional structure of the A$\beta_{(10-35)}$ fibril.

Results

Electron Microscopy. The more complex models of Aβ fibril formation, specifically those which place the hydrophobic C-termini in the core of the fibrils,[10] predict that PEG attachment

(7) (a) Lee, J. P.; Stimson, E. R.; Ghilardi, J. P.; Mantyh, P. W.; Lu, Y. A.; Felix, A. M.; Llanos, W.; Behbin, A.; Cummings, M.; Van Criekinge, M.; Timms, W.; Maggio, J. E. *Biochemistry* **1995**, *34*, 5191−5200. (b) Esler, W. P.; Stimson, E. R.; Ghilardi, J. P.; Lu, Y. A.; Felix, A. M.; Vinters, H. V.; Mantyh, P. W.; Lee, J. P.; Maggio, J. E. *Biochemistry* **1996**, *35*, 13914−13921. (c) Benzinger, T. L. S.; Gregory, D. M.; Burkoth, T. S.; Miller-Auer, H.; Lynn, D. G.; Botto, R. E.; Meredith, S. C. *Proc. Natl. Acad. Sci. U.S.A.* **1998**, *95*, 13407−13412. (d) Gregory, D. M.; Benzinger, T. L. S.; Burkoth, T. S.; Miller-Auer, H.; Lynn, D. G.; Meredith, S. C.; Botto, R. E. *Solid State Nucl. Magn. Reson.* **1998**, *13*, 149−166. (e) Benzinger, T. L. S.; Gregory, D. M.; Burkoth, T. S.; Miller-Auer, H.; Lynn, D. G.; Botto, R. E.; Meredith, S. C. *Biochemistry* **2000**, *39*, 3491−3499. (f) Lynn, D. G.; Meredith, S. C. *J. Struct. Biol.* **2000**, in press.

(8) Gregory, D. M.; Mehta, M. A.; Shiels, J. C.; Drobny, G. P. *J. Chem. Phys.* **1997**, *107*, 28−42.

(9) Burkoth, T. S.; Benzinger, T. L. S.; Jones, D. N. M.; Hallenga, K.; Meredith, S. C.; Lynn, D. G. *J. Am. Chem. Soc.* **1998**, *120*, 7655−7656.

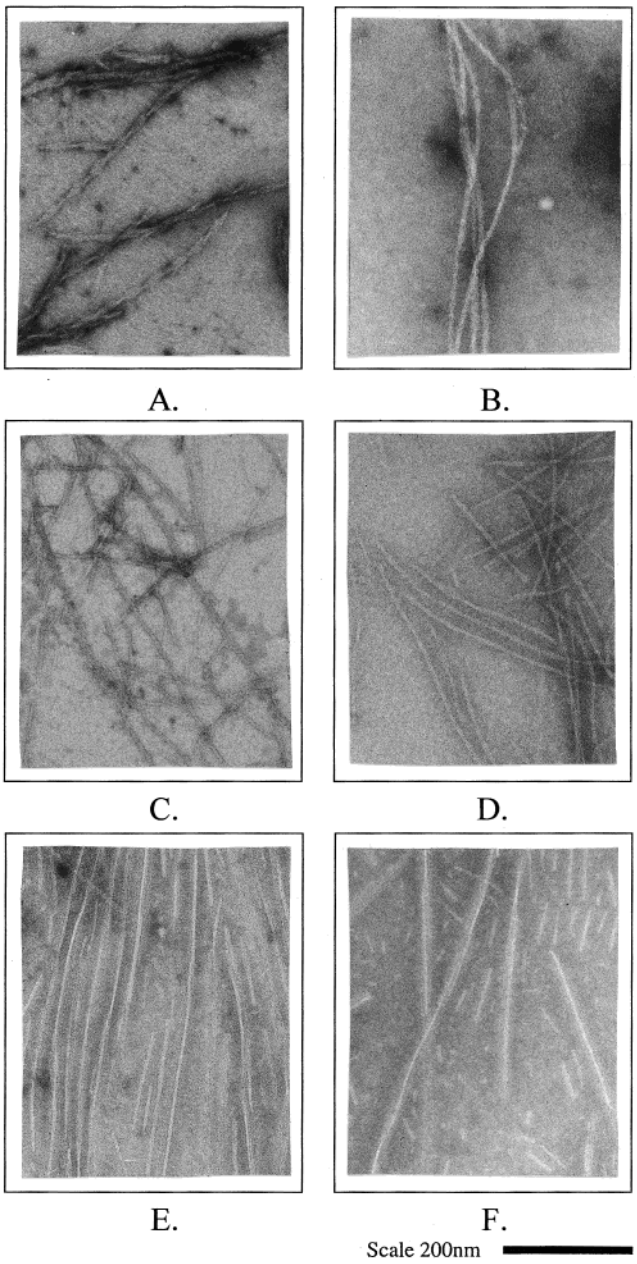

Figure 2. Electron micrographs of A$\beta_{(10-35)}$ titrated with Aβ-PEG at pH 5.7: (A) 100% A$\beta_{(10-35)}$, (B) 10:1 A$\beta_{(10-35)}$:Aβ-PEG, (C) 6:3 A$\beta_{(10-35)}$:Aβ-PEG, (D) 1:1 A$\beta_{(10-35)}$:Aβ-PEG, (E) 1:4 A$\beta_{(10-35)}$:Aβ-PEG, and (F) 100% Aβ-PEG.

would disrupt fibril formation and/or form a different structure. EM was used to examine the morphology of fibrils formed from the two synthetic peptides as well as mixtures of each (Figure 2). The ratio of A$\beta_{(10-35)}$ to A$\beta_{(10-35)}$-PEG was adjusted while keeping the total peptide concentration constant. Fibrils composed entirely of A$\beta_{(10-35)}$ contained largely twisted, paired fibrils, ~90 Å by ~160 Å across the narrowest and thickest dimensions, with a superhelical repeat distance of ~1100 Å, and occasional monomeric fibrils ~80 Å in diameter (Figure 2A). As the A$\beta_{(10-35)}$-PEG component was increased, there was less lateral self-association of the fibrils (Figure 2B−E). In addition, the EM staining of the fibrils became more diffuse and a halo around the fibrils was visible. A$\beta_{(10-35)}$-PEG fibrils (Figure 2E) were not paired and had diameters of >80 Å. These observations are consistent with A$\beta_{(10-35)}$-PEG and A$\beta_{(10-35)}$ randomly distributing themselves within the fibrils maintaining the PEG block localized to the surface of the A$\beta_{(10-35)}$ fibril to prevent fibril−fibril association.[9] By extension, the hydrophobic C-terminus of A$\beta_{(10-35)}$ would also be localized to the edge of a monomeric fibril and thus exposed to solvent in the absence of pairing. For this reason, in the absence of PEG, single filaments would associate and entangle so as to sequester the hydrophobic edge from solvent.

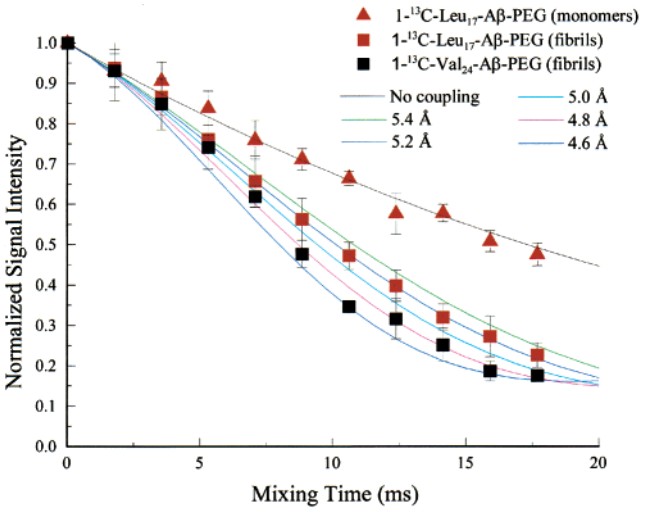

Figure 3. Analysis of the solid-state NMR DRAWS experiment on 1-^{13}C-Leu$_{17}$-Aβ-PEG and 1-^{13}C-Val$_{24}$-Aβ-PEG before and after fibril formation using a series of mixing times from 0 to 22 ms. At each mixing time, the carbonyl peak was integrated and normalized to the first data point (mixing time = 0) to allow comparison between samples. Values shown are the mean ± one standard deviation for 10 mg of lyophilized fibrils (squares, $n = 5$) and 10 mg of nonfibrilized ether precipitate (triangles, $n = 5$) compared to numerical simulations of no interaction (triangles). Simulations are for 5.4 (green), 5.2 (blue), 5.0 (turquoise), 4.8 (red), and 4.6 Å (blue) interactions.

Solid-State NMR Analyses. The solid-state NMR DRAWS experiments allowed the peptide arrangement within the A$\beta_{(10-35)}$-PEG fibril to be analyzed directly. In A$\beta_{(10-35)}$-PEG fibrils,[4] prepared with either 1-^{13}C-Leu$_{17}$ or 1-^{13}C-Val$_{24}$ isotopic labels, carbonyl−carbonyl distances were fit as a repeating array of 5.2(±0.3) and 4.8(±0.3) Å respectively, as shown in Figure 3. As with the control nonfibrilized A$\beta_{(10-35)}$ peptides,[7c−f] A$\beta_{(10-35)}$-PEG samples that were not allowed to fibrilize showed no measurable Leu$_{17}$-Leu$_{17}$ or Val$_{24}$-Val$_{24}$ inter-peptide dipolar coupling. Analysis of structures in the Brookhaven Protein Data Bank had previously established that only β-structures could readily accommodate this carbonyl−carbonyl distance between strands,[7c] and only homogeneous preparations could give such precision in the NMR distance measurements. Moreover, the spacing of these labels across the peptide at residues 17 and 24 established that all the peptides existed as parallel strands with residues in exact register. Thus, the A$\beta_{(10-35)}$-PEG block copolymer forms fibrils whose self-assembly is dominated by the peptide block, and which maintain the basic interpeptide alignment of the A$\beta_{(10-35)}$ fibril.

Small-Angle Neutron Scattering. The improved solubility and single stranded character of the A$\beta_{(10-35)}$-PEG fibril made

(10) Fraser, P. E.; McLachlan, D. R.; Surewicz, W. K.; Mizzen, C. A.; Snow, A. D.; Nguyen, J. T.; Kirschner, D. A. *J. Mol. Biol.* **1994**, *244*, 64−73. Lansbury, P. T., Jr.; Costa, P. R.; Griffiths, J. M.; Simon, E. J.; Auger, M.; Halverson, K. J.; Kocisko, D. A.; Hendsch, Z. S.; Ashburn, T. T.; Spencer, R. G.; Tidor, B.; Griffin, R. G. *Nat. Struct. Biol.* **1995**, *2*, 990−998. Malinchik, S. B.; Inouye, H.; Szumowski, K. E.; Kirschner, D. A. *Biophys. J.* **1998**, *74*, 537−545. Lazo, N. D.; Downing, D. T. *Biochemistry* **1998**, *37*, 1731−1735.

it far easier to analyze in solution. The differential neutron scattering cross-section, $I(Q)$, in the absence of interparticle correlation, is given by

$$I(Q) = N_p \cdot V_p^2 \cdot (\rho_p - \rho_r)^2 F(Q) \quad (1)$$

where N_p is the number of particles per unit volume, V_p is the volume of the particles, $F(Q)$ is the form factor describing the shape of the particles, and ρ_p and ρ_r are the neutron scattering length density of the particle and the solvent, respectively. The scattering length density ρ for any system can be calculated using eq 2

$$\rho = N_A d(\sum b_i / \sum M_i) \quad (2)$$

where b_i and M_i are the neutron scattering length and mass of the ith atom in the system, respectively, d is the macroscopic density of the system, and N_A is Avogadro's number. The difference in the square of the scattering length densities of the particle and the matrix is known as the contrast. $I(Q)$ will be zero if the scattering length density of the particle is equal to that of the solvent. Since the scattering length densities of H_2O, D_2O, and PEG are -0.56×10^{10}, 6.34×10^{10}, and 0.57×10^{10} cm^{-2}, respectively, the coherent scattering from PEG can be eliminated[12] if a solvent containing 16% D_2O is used in the buffer for dispersing the A$\beta_{(10-35)}$-PEG.

The measured differential neutron scattering cross-section for the A$\beta_{(10-35)}$-PEG fibril was interpreted initially using a modified Guinier analysis[4,11,12] for a rod by plotting $\ln[Q \cdot I(Q)]$ versus Q^2. Rodlike particles give rise to a linear region in the modified Guinier plot in the low Q region ($Q \cdot R_c < 1$) where the cross-sectional radius of gyration of the rod, R_c, can be derived from the negative slope of the straight line by the relation $R_c^2 = -2 \times$ slope.[13] The modified Guinier analysis of the measured data for A$\beta_{(10-35)}$-PEG in 16% D_2O at pH 5.6 gave a radius, $R = \sqrt{2} \cdot R_c$, of 38 ± 3 Å for the A$\beta_{(10-35)}$ portion of the A$\beta_{(10-35)}$-PEG fibril (Figure 4). The mass per unit length of the fibril can be determined from $I_c(0)$, which corresponds to the y-intercept of the modified-Guinier plot for rodlike forms, using eq 3.

$$M_L = (I_c(0) \times 10^3) d^2 N_A / [\pi c (\rho_p - \rho_s)^2] \quad (3)$$

Here, M_L corresponds to the molar mass per unit length of the rod, N_A is Avogadro's number (6.022×10^{23}/mol), and the scattering length density of 16% D_2O, ρ_s, is 0.547×10^{10} cm^{-2}. Because PEG3000 does not contribute to the measured differential scattering cross-section, the relevant concentration c (g/L) is that of the peptide only in the 11.5 g/L A$\beta_{(10-35)}$-PEG solution, and is 5.67 g/L.

For the scattering length density of the peptide ρ_p, the chemical formula for the peptide block is $C_{133}H_{204}N_{34}O_{36}$ with a MW = 2855. However, there are 31 exchangeable protons in A$\beta_{(10-35)}$, and in 16% D_2O, on average 5 of them will be exchanged with solvent. Hence, the experimental chemical formula for Aβ_{10-35} in 16% D_2O is $C_{133}H_{199}D_5N_{34}O_{36}$. Therefore, the peptide ρ_p, calculated using eq 2 with a density, based on partial specific volume of a β-helix (0.744 cm^3/g) of 1.35 g/mL, is 1.995×10^{10} cm^{-2}. We have used this value in eq 3 for the determination of M_L for the rodlike particles in the A$\beta_{(10-35)}$-PEG solution from $I_c(0)$.

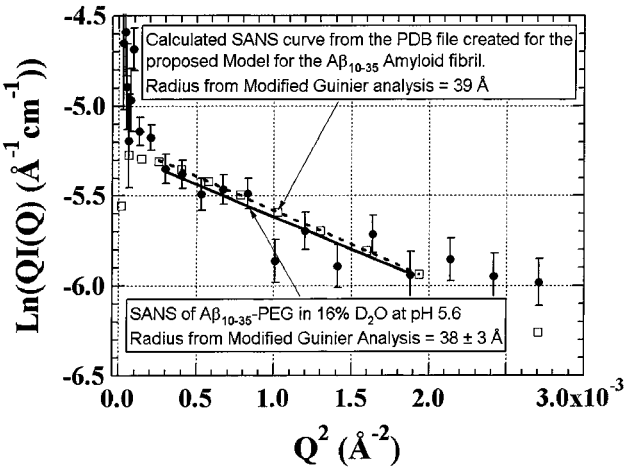

Figure 4. Modified Guinier plot for a rod of the measured SANS data for the A$\beta_{(10-35)}$-PEG at pH 5.6 in 16% D_2O buffer: the linear fits (solid line) for the measured data (filled circles) and the SANS curve calculated for the model proposed for the fibril (open squares and dotted line).

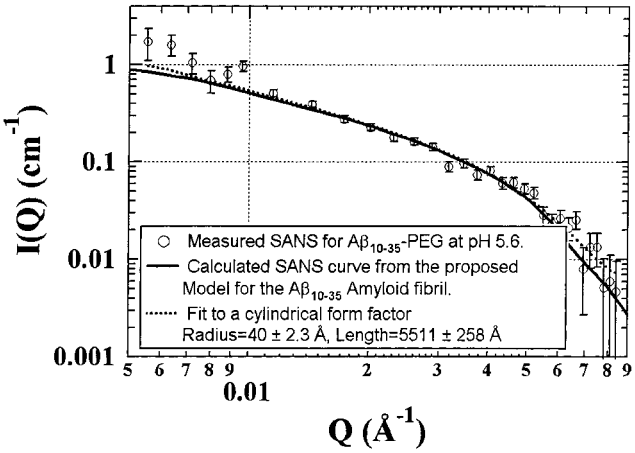

Figure 5. Measured SANS data for the A$\beta_{(10-35)}$-PEG at pH 5.6 in 16% D_2O buffer along with the fit to the data using the form factor for a long cylinder (eq 4) and the SANS curve calculated using the coordinates generated for the proposed model using CRYSON. The latter seems to fit the data better in the high Q region.

Fibrils prepared from a 11.5 mg/mL A$\beta_{(10-35)}$-PEG solution gave an $I_c(0)$ value of $1.23 \times 10^{-2} \pm 5 \times 10^{-4}$ cm^{-1} $Å^{-1}$. Using these values in eq 3, M_L was determined to be 3686 ± 150 Da/Å. A separate A$\beta_{(10-35)}$-PEG fibril prepared from a 5.10 g/L solution (2.49 g/L of peptide when corrected for the PEG block) gave an $I_c(0)$ of $5.16 \times 10^{-3} \pm 5 \times 10^{-4}$ cm^{-1} $Å^{-1}$ and a calculated mass per unit length of 3453 ± 340 $\Delta\alpha$/Å. A single β-sheet, with an average peptide−peptide distance of 5 Å, as established by the solid-state NMR studies of A$\beta_{(10-35)}$, predicts a mass per unit length of 572 Da/Å. Thus, the average M_L from SANS for the two different samples in 16% D_2O indicates a structure having 6.2 ± 0.6 such sheets making up the fibrils.

We have also modeled the SANS data for the A$\beta_{(10-35)}$-PEG solution in 16% D_2O with the form factor for an infinitely long cylinder,[14] eq 4. The fit to the data shown in Figure 5 is quite reasonable and corresponds to a cylinder with a radius = 40 ±

(11) Thiyagarajan, P.; Burkoth, T. S.; Urban, V.; Seifert, S.; Benzinger, T. L. S.; Morgan, D. M.; Gordon, D.; Meredith, S. C.; Lynn, D. G. *J. Appl. Crystallogr.* **2000**, *33*, 535−539.

(12) Thiyagarajan, P.; Chaiko, D. J.; Hjelm, R. P., Jr. *Macromolecules* **1995**, *28*, 7730−7736.

(13) Porod, G. In *Small Angle X-ray Scattering*; Glatter, O., Kratky, O., Eds.; Academic Press: New York, 1982; Chapter 2.

(14) Neugebauer, T. *Ann Phys.* (*Leipzig*) **1943**, *42*, 509−533.

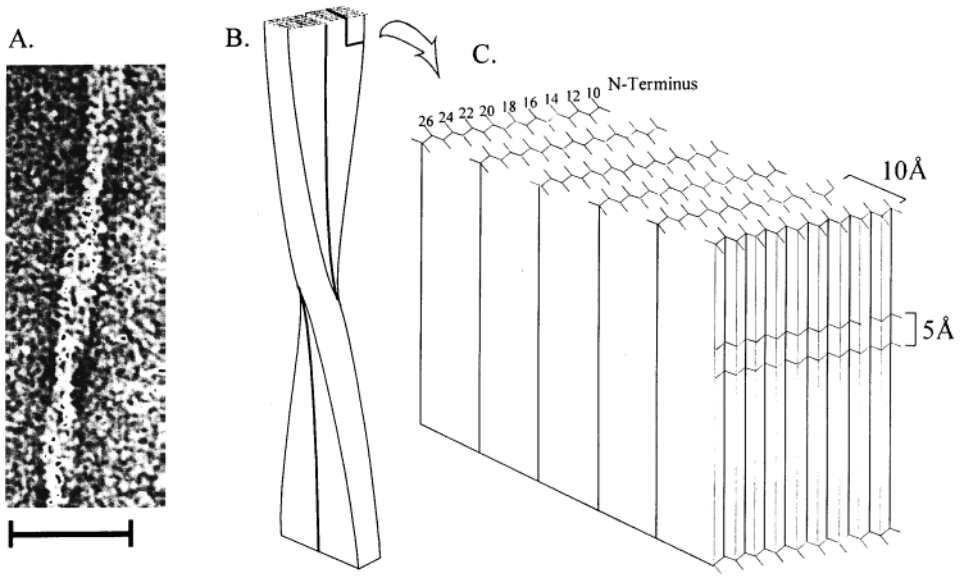

Figure 6. Three-dimensional structure of Aβ (10−35). (A) Electron micrograph of a typical paired helical fiber observed for Aβ(10−35) at pH 7.4 (scale 30 nm). (B) Structure of the paired fibrils incorporating the 1100 Å repeat composed of 220 β-strands, each with a 1.6° offset to define the twist of the β-helices. Orienting the peptides in parallel and in register would place the hydrophobic C-terminal amino acids entirely along one edge of the β-sheet driving their association. (C) Expansion of the six laminated sheets. The strands are H-bonded and held roughly 5 Å apart within the β-sheet. The H-bonds are oriented collinear with the fibril axis. The packing of the amino acid side chains, oriented perpendicular to the fibril axis, results in the 10 Å separations between the individual sheets.

2.3 Å and a length = 5511 ± 258 Å. The radius value from the fit agrees well with that from the modified Guinier analysis.

$$F_C = F_{CS}(Q,R)F_L(Q,L) \tag{4}$$

where

$$F_{CS}(Q,R) = \left[\frac{2J_1(QR)}{QR}\right]^2 \tag{5}$$

$$F_L(Q,R) = \frac{2Si(QL)}{QL} - 4\sin^2\left(\frac{QL}{2}\right)\frac{1}{Q^2L^2} \tag{6}$$

and

$$Si(x) = \int_0^x \frac{\sin t}{t}\,dt \tag{7}$$

The large uncertainty in the length of the cylinder fit is due to the limited Q_{min} reached in the SANS measurement. Deviation from a straight line in the lowest Q^2 region (Figure 4) may be due to the presence of small amounts of fibril−fibril association. A similar deviation is seen in Figure 5 in the low Q region where the experimental data bend upward, again consistent with higher aggregations. The PEG block therefore dramatically slows, but does not completely prevent, fibril−fibril self-association.

Structure Model. A fully extended Aβ(10−35) peptide, stacked as the in register β-sheet determined by the solid-state NMR experiments, would be ∼82 Å in length. The stacking of these peptides into an extended parallel β-sheet propagating along the fibril axis would give an extended, or β-helix conformation (Figure 6A), a structure proposed to be a common feature of amyloid fibrils,[15] and define one dimension of the fibril.

Fibril thickness, established as a stack of six β-helices by the SANS mass per unit length determinations, must be ∼60 Å due to the 10 Å close pack sheet-to-sheet distance of β-helices.[15] The EM dimensions, the CD analysis of the equilibrium association of Aβ(10−35)-PEG,[9] as well as the transglutaminase cross-linking of both Aβ(10−35)-PEG and Aβ(10−35)[7c,9] are consistent with six laminated β-sheets.

A structure consisting of a lamination of six parallel sheets, positioned 10 Å apart, would give a rectangular rod having dimensions of 82 × 60 Å. A parallel orientation between the laminates would position Gln_{15} and Lys_{16} side chains for cross-linking between sheets as observed in both Aβ(10−35)-PEG and Aβ(10−35) fibrils.[7c,9] While a parallel orientation would place the ^{13}C-labeled carbonyls in register between laminates, the ∼10 Å spacing is a distance too great to contribute to the dipole−dipole coupling in the NMR experiment. Such an orientation would also place the PEG block of Aβ(10−35)-PEG spiraling along the hydrophobic face of the fibril, consistent with the SANS experiments,[4] and the observed reduction in fibril−fibril association.[9] Indeed, the paired fibrils are not observed by EM and are radically reduced in SANS analyses following covalent attachment of PEG at the C-terminus. Building on this model, the super helical twist shown in Figure 6A can be assigned as an antiparallel pair of β-helical bundles with the measured dimensions of 180 × 70 Å as shown in Figure 6B,C. The average duplex pitch of ∼1100 Å seen in EM, composed of peptides within each sheet spaced at 5 Å intervals (Figure 6C), predicts the individual β-strands are offset by a rather shallow 1.6°/Aβ(10−35) peptide.

To further evaluate this structure, the SANS data were fit using the atomic coordinates of the backbone atoms predicted by Figure 6C. The calculated SANS curve in Figure 5 was obtained using CRYSON software, a package developed for calculating the SANS scattering intensities from protein crystal structure data.[16] The calculated curve agrees quite well at $Q > 0.008$ Å^{-1}. Furthermore, the modified Guinier analysis of the

(15) Cohen, F. E. *Science* **1993**, *260*, 1444−5. Jurnak, F,; Yoder, M. D.; Pickergill, R.; Jenkins, J. *Curr. Opin. Struct. Biol.* **1994**, *4*, 802−6. Blake, C.; Serpell, L. *Structure* **1996**, *4*, 989−998. Harper, J. D.; Lieber, C. M.; Lansbury, P. T., Jr. *Chem. Biol.* **1997**, *4*, 951−959. Sunde, M.; Serpell, L. C.; Bartlam, M.; Fraser, P. E.; Pepys, M. B.; Blake, C. C. *J. Mol. Biol.* **1997**, *273*, 729−39. Teplow, D. B. *Amyloid* **1998**, *5*, 121.

(16) Svergun, D. I.; Barberato, C.; Koch, M. H. J. *J. Appl. Crystallogr.* **1995**, *28*, 786−773.

calculated SANS data gives a cross-sectional radius of 39 Å which is consistent with the experimental radius of 38 ± 3 Å. Although the χ^2 values for the cylinder fit and the fibril model to the SANS data are quite similar, the agreement between the model and experimental data seems to be slightly better in the high Q region where details of the local structure are more apparent.

Discussion

The number of diseases known to be associated with amyloid deposits continues to grow, and the most well-known of these, AD, is already predicted to have a dramatic effect on the elderly population and health care costs in the coming decades. Developing strategies and methods for determining the structure of the amyloid fibrils will be critical to defining the mechanisms of self-aggregation and uncovering targets for therapeutic intervention. Here we report a combination of physical and chemical methods that have allowed critical elements of the structure of the A$\beta_{(10-35)}$ fibril to be determined.

The proposed model for the A$\beta_{(10-35)}$ fibril incorporates elements that appear to be common in many other amyloids.[15] In fact, a general structural model proposed 25 years ago[17] was based on polysaccharide dye binding agents, specifically I_2 and Congo Red, EM analyses,[18] and the initial X-ray diffraction results.[19] It was the common staining of these fibrils with polysaccharide dyes that led initially to the term "amyloid",[20] and the analogy with the organized arrays of the cellulose fibrils that suggested a related organized array for the amyloid peptides. Since then, this model has been extended, but generally with the assumption, implicit or explicit, that the β-sheet structure was antiparallel.

The most well determined feature of the A$\beta_{(10-35)}$ fibril is the in-register, parallel β-sheet arrangement that exists between the individual peptides. This feature is based on solid state NMR measurements of the dipolar coupling between spin labels brought into proximity to one another by fibril formation. Especially where the shorter interstrand distances are concerned, but also more generally, these measurements are consistent only with a relatively homogeneous distribution of interpeptide distances, whether in frozen solution or in lyophilized solids.[7c,d] Even attachment of the large bulky PEG block did not disrupt the favorable free energy driving the in-register parallel β-sheet self-assembly of A$\beta_{(10-35)}$.

The SANS experiments enabled direct measurements of the mass per unit length of the fibrils and established that six such β-sheets laminated as a β-helix was sufficient to generate the backbone atom coordinates necessary to model the observed scattering densities. While these data supported a 10 Å spacing between the laminated sheets, the relative orientation of the sheets was not addressed. The t-glutaminase cross-linking reactions[7c,9] between Glu_{15}-Lys_{16} in a β-sheet arrangement predicted that these sheets are laminated parallel with respect to one another, but neither the NMR nor the SANS experiments addressed this aspect directly. β-Helices are often composed of homologous repeating sequences, most notably Tyr, Phe, and bulky hydrophobic amino acids (Leu, Ile, Val).[21] In the A$\beta_{(10-35)}$ parallel lamination, the i, $i+1$ paired adjacent amino acids, most notably His_{13}-His_{14}, Leu_{17}-Val_{18}, Phe_{19}-Phe_{20}, and Ile_{31}-Ile_{32}, would result in repeating aromatic and/or aliphatic stacks along both faces of every β-sheet and in register with the adjacent sheets. The central core of hydrophobic residues, LVFFA, apparently critical for fibril formation in Aβ peptides, also constitutes a surface that would be expected to stabilize sheet−sheet stacking, but only if the sheets are arrayed in parallel. Further experiments to evaluate laminate energetic stabilities are being pursued.

A$\beta_{(10-35)}$-PEG is unique among the Aβ derivatives in that its self-assembly into fibrils is freely reversible with both changes in concentration and pH.[9] The dramatic pH dependence for fibril formation can be understood in this structure and attributed to the charged side chain interactions between laminates. For example, His_{13} and His_{14}, while on opposite faces of a single β-sheet, would directly interact with the respective His_{14} and His_{13} residues of the adjacent, laminated sheet or sheets. The degree of protonation and/or the presence of metal ions would alter laminate stability. In that regard, divalent metal ions, e.g. Zn^{2+}, have been shown to increase the rate of fibril formation at least of the full length Aβ peptides.[22] Such coordination of Zn^{2+} by histidines on facing β-sheets within a β-helix has been observed in the crystal structure of carbonic anhydrase.[23] Our preliminary evidence also suggests that Zn^{2+} dramatically alters both the rate of A$\beta_{(10-35)}$-PEG fibrilization as well as the resulting fibril structure.

In summary, these data have established essential structural elements of the A$\beta_{(10-35)}$ fibril, one of the largest paracrystalline molecular assemblies to be determined at this level of resolution. The fibril is an elegantly simple organization of peptides arrayed as parallel in-register β-sheets with up to six of these sheets laminated in an apparent parallel array along the fibril axis. This arrangement predicts the dimensions of 82 × 60 Å, consistent with that seen in EM and X-ray and neutron scattering for a fibril that propagates for well over 5000 Å. Each individual sheet has a very shallow deviation from planarity, a deviation that dictates the helical twist, and possibly the laminate number, in the fibril. This twist is apparent in paired fibrils where the super-helical pitch of an antiparallel organization results from an association along their hydrophobic C-terminal faces. Such a structural design of paired helices of opposite antiparallel orientation, spiraling to protect a hydrophobic interior, is one of Nature's most common and fundamental designs, most apparent in Watson−Crick DNA duplexes. The perspective provided by this structure and the methods developed for its characterization should be relevant to any self-assembling array that are typified by, but certainly not the sole domain of, the amyloidogenic peptides and proteins.

Materials and Methods

Syntheses. A$\beta_{(10-35)}$-PEG containing either 1-^{13}C-Leu or 1-^{13}C-Val was synthesized using standard fluorenyl-methoxy carbonyl protocols on PAP Tenta-Gel (Rapp Polymere) to introduce the label at position 17 or 24.[9] Cleavage by TFA and deprotection yielded a linear PEG 3000 covalently bound to the carboxyl terminus of the peptide. Peptide purity, determined by synthetic coupling yields and reverse phase HPLC of CNBr cleavage products, was >96%. Molecular masses of all peptides were verified by MALDI-TOF mass spectroscopy.

Solid-State NMR. A$\beta_{(10-35)}$-PEG fibrils were prepared as previously described,[7c] and CP/MAS ^{13}C NMR experiments were performed on a Bruker Avance DSX spectrometer at 50.3 MHz using the DRAWS sequence.[8] Spectra were acquired on 10-mg samples with >500 scans

(17) Cooper, J. H. *Lab. Invest.* **1974**, *31*, 232−238.
(18) Glenner, G. G.; Keiser, H. R.; Bladen, H. A.; Cuatrecasas, P.; Eanes, E. D.; Ram, J. S.; Kanfer, J. N.; DeLellis, R. A. *J. Histochem. Cytochem.* **1968**, *16*, 633−644.
(19) Gueft, B. *Mt. Sinai J. Med. N.Y.* **1972**, *39*, 91−102.
(20) Virchow, R. *Virchows Arch.* **1854**, *8*, 140.
(21) Nesloney, C. L.; Kelly, J. W. *Bioog. Med. Chem.* **1996**, *4*, 739−766.
(22) Bush, A. I.; Pettingell, W. H.; Multhaup, G.; Paradis, M. D.; Vonsattel, J. P.; Gusella, J. F.; Beyreuther, K.; Masters, C. L.; Tanzi, R. E. *Science* **1994**, *265*, 1464−1467.
(23) Kisker, C.; Schlindelin H.; Alber, B. E.; Ferry, J. G.; Rees, D. C. *EMBO J.* **1996**, *15*, 2323−2330.

for the fibril samples and >1800 scans for the nonfibrilized control sample of 1-^{13}C-Leu$_{17}$-A$\beta_{(10-35)}$PEG or 1-^{13}C-Val$_{24}$-A$\beta_{(10-35)}$-PEG. Hexamethylbenzene (8−12 mg) served as internal control. Samples were spun at 4525(±3) Hz, the ^{13}C RF power level was 38.5 kHz, the ^{1}H decoupling level was 120 kHz, and the spectra were processed and analyzed as previously described.[7d] Virtually all β-sheet carbonyl chemical shifts are superimposable at δ 171 ppm in the solid-state NMR experiment and the signal attributable to the unlabeled amino acids was subtracted from the total signal as previously described.[7d]

Simulated data were created by numerical calculation using a density matrix approach.[7d] The input parameters to the numerical calculation program included the chemical shift tensor (CSA) elements for the spin-$^{1}/_{2}$ nuclei, the dipolar coupling strengths, Euler angles which rotate the CSA tensors from the molecular frame to their respective principal axis systems, an initial density matrix $p(0)$, an observable, and any relevant relaxation parameters. In this work, the Euler angles were set to zero, as it was determined that they had a negligible effect on the simulated curves. The CSA parameters were taken from Ye et al.[24] The time increment was typically 2−3 ms. Relaxation effects were modeled by multiplying the single quantum density matrix elements by an exponential factor at the end of each time increment. Data from the nonfibrilized sample were used to determine the appropriate single quantum relaxation constant. The program also performs a powder average of 2000 randomly selected crystallite orientations.

Electron Microscopy. Samples of A$\beta_{(10-35)}$/A$\beta_{(10-35)}$-PEG were prepared for EM by dissolving dry peptide to 2 mM in water containing 0.1% NaN_3 (pH ∼3.0). The samples were mixed, centrifuged for 15 min at 14 000 X g, and incubated for 1 h. The mixtures were then diluted to 1 mM in phosphate buffer at pH 5.6 and allowed to stand at room temperature for 3 days. Samples were applied to a glow discharge 400 mesh carbon coated support film, followed by staining with 1% uranyl acetate. Micrographs were recorded using a Philips EM 300 at magnifications of 100 000, 45 000, and 10 000.

Small-Angle Neutron Scattering. SANS experiments were performed at the time-of-flight small-angle diffractometer (SAD) at the Intense Pulsed Neutron Source of Argonne National Laboratory.[25] Pulsed neutrons were detected at a fixed sample-to-detector distance of 1.54 m with a 64 × 64 array position sensitive gas filled 20 × 20 cm^2 area detector, and the wavelengths λ 0.5−14 Å were measured with time-of-flight by binning the pulse to 67 constant $\Delta\lambda/\lambda = 0.05$ time channels. This instrument provides a useful range of scattering vector ($Q = 4\pi \sin(\theta)/\lambda$), where θ is half the scattering angle and λ is the wavelength of the probing neutrons) of 0.005−0.25 Å^{-1} in a single measurement. A$\beta_{(10-35)}$ (4.6 g/L) and A$\beta_{(10-35)}$-PEG (11.5 g/L) in 16% D_2O buffer at pH 5.6 were analyzed in 1 mm quartz cells. Each of the samples and the buffer solutions in 16% D_2O (low contrast for protein and no contrast for PEG) were measured for about 20 h. The scattering data were corrected for the background from the instrument, the sample cell, and the solvent and the differential scattering cross-section was placed on an absolute scale in the units of cm^{-1}.[28]

Acknowledgment. We thank the Argonne National Laboratory-University of Chicago Collaborative Grants Program (R.E.B., D.G.L., S.C.M., and P.T.) and the NIH (R21 RR 12723, D.G.L.) for support, and the NIH (5 T32 HL07327, T.S.B.; 5 T32 GM07281, T.L.S.B.), the American Federation for Aging Research (T.L.S.B.), and the American Foundation for Aging Research (T.L.S.B.) for fellowships. This work was performed under the auspices of the Office of Basic Energy Sciences, Division of Chemical and Materials Sciences, U.S. Department of Energy, under contract number W-31-109-ENG-38. This work benefited from the use of facilities in the Intense Pulsed Neutron Source.

JA000645Z

(24) Ye, C.; Fu, R.; Hu, J.; Hou, L.; Ding, S. *Magn. Reson. Chem.* **1993**, *31*, 699−704.

(25) Thiyagarajan, P.; Epperson, J. E.; Crawford, R. K.; Carpenter, J. M.; Kilppert, T. E.; Wozniak, D. G. *J. Appl. Crystallogr.* **1997**, *30*, 280−293.